

Part II: METHODOLOGY

NON-ERGODIC PROBABILISTIC SEISMIC HAZARD METHODOLOGY USING PHYSICS-BASED GROUND MOTION PREDICTION THE CASE OF L'AQUILA, ITALY

JEDIDIAH JOEL AGUIRRE^{1,2}, BRUNO RUBINO¹, MAURIZIO VASSALLO³, GIUSEPPE DI GIULIO³
AND FRANCESCO VISINI⁴

¹Università Degli Studi Dell'Aquila 67100 L'Aquila, Italy

²University of the Philippines 4031 Los Baños, Laguna, Philippines

³Istituto Nazionale di Geofisica e Vulcanologia – Sezione dell'Aquila 67100 L'Aquila, Italy

⁴Istituto Nazionale di Geofisica e Vulcanologia – Sezione di Pisa 56125 Pisa, Italy

(received: 4 January 2020; revised: 9 February 2020; accepted: 15 March 2020; published online: 1 April 2020)

DOI: https://doi.org/10.34808/tq2020/24.2/a_part2

4. PSHA Methodology

In the previous Sections, the need for the estimation of the seismic hazard was presented at the beginning, then the basic notions of seismology were discussed, and lastly, the solution to the elastodynamic equation was examined for the ground motion prediction. Hence, the probabilistic approach of estimating the seismic hazard level will be presented in this Section. Kramer's [1] outline of PSHA was used to discuss the methodology with the exception of using the Physics-based Ground Motion Prediction to abandon the ergodic assumption in conducting PSHA. Readers who need a review in the fundamental concepts in probability are referred to Appendix A to this paper.

4.1. Delineation of Seismic Sources

All significant seismic sources that can produce strong ground shaking will be considered when conducting a PSHA. For this study, active fault source models were used extensively from Valentini, Visini, and Pace [25] and Valentini et. al. [24] since fault geometry parameters were provided in their papers, and the shapefiles of fault traces were obtained online as per recommendation of Valentini, Visini, and Pace [25] which is available for public use. Figure fig4.1 and Table 3 show the fault traces located within a 100km radius from the city of L'Aquila as well as the master fault associations of these fault traces based on Valentini, Visini, and Pace [25], both of which are mapped using ArcGIS Pro from the shapefile obtained online. Table 2 shows the fault parameters needed for a seismic hazard analysis such as the fault length (in km), the dip angle (in degrees), the seismogenic thickness (ST in km), the minimum and maximum slip rates observed (SR_{min} , SR_{max} in mm/year), the observed earthquake event M_{obs} and its standard deviation, and the recent instrumental recording of the year of occurrence.

Table 2 shows that the Fucino fault is the longest with a length of 45.9km, while Velino is the shortest with a length of 11.5km. All the faults have a dip angle less than 90^0 , which suggests that all the faults are dip-slip faults. All faults have fault traces located on the surface [25], which implies that the given seismogenic thicknesses in Table 2 is the deepest part of the fault for all sources. For slip rates, Leonessa and Pizzalto-Cinque Miglia have the smallest slip rates of 0.1mm/year,

while Fucino has the biggest slip rate of 1.4mm/year. The slip rate is the annual movement of the fault which imposes shear stresses on the fault causing an elastic build-up of strain energy [1].

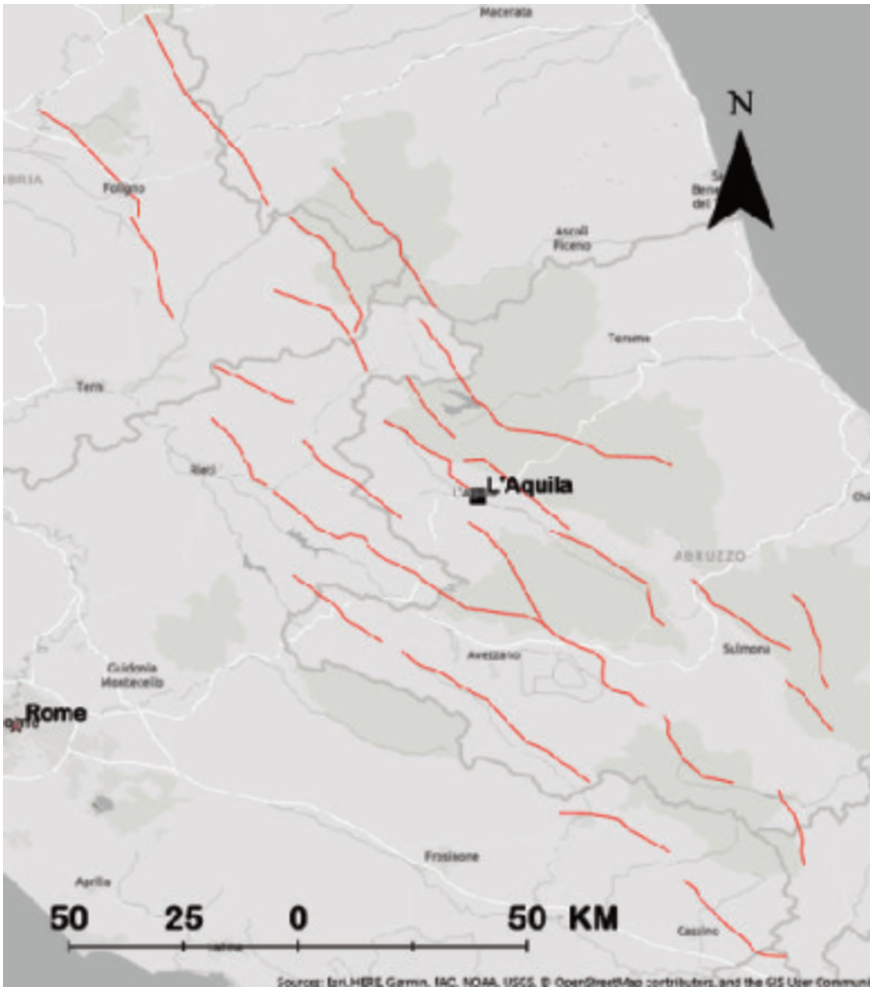


Figure 18. Fault traces located at a radius of 100 km from L'Aquila

Source: Valentini, Visini and Pace, 2017 [25]

Earthquake occurrences were recorded only by several fault sources, which are Colfiorito, Fucino, Mount Vettore, Mount Bove, Paganica, Pizzoli-Pettino, Rieti, Salto Valley, Sora, Umbra Valley North and the South segments, and Velino, according to Table 2. Therefore, additional information coming from the paleoseismological records and other literature which can provide the fault activity was required to fully characterize a seismic source.

Historical seismicity and paleoseismological records were extracted from various literature sources to characterize the fault activity from Valentini et

al. [24] and Valentini, Visini, and Pace [25]. For the purpose of showing such information, Table 2 presents the historical, instrumental, and paleoseismological records of past earthquake occurrences in all the faults considered in this study. The data was used by Valentini et al. [24] for estimating the recurrence period of earthquakes by considering the past earthquake occurrences the values of which were used to calculate the seismic moment in each fault.

It follows from Table 2 that all the seismic sources show evidence of fault activity even before the 20th century except for Carsoli, Cassino, Leonessa, Liri, Maiella, Marsicano, Montereale, and Sella di Corno. For these faults that have no earthquake association, additional assumption was used to characterize the fault activity to be discussed later.

4.2. Distance Calculations

After identifying all the potential seismic sources that can significantly contribute to the seismic hazard on a site, the distances of all possible earthquake scenarios must be obtained. These distances were used as lengths of wave propagations for the ground motion prediction.

In this study, ArcGIS Pro was used to discretize all the active fault sources into 100 equal areas and the Calculate Geometry Functions of the software were used to obtain coordinates of the centroid in the latitude and longitude coordinates. The distances from each centroid were obtained with the coordinates of L'Aquila at 42.3498° N, 13.3995° E. Next, the distances obtained were subdivided into 10 equally spaced bins. Then, a histogram showing the number of distances that fall into a certain bin was made for each seismic source, the probability mass functions of which are presented in Appendix B to this paper.

5. Magnitude-Frequency Distributions

The next thing to come after the calculations of source-to-site distances is the modeling of the uncertainty in the size of earthquakes. Before doing this, usually the maximum magnitude that a fault can produce must be computed first along with the uncertainty to produce the PDF of the magnitude. Then, the associated activity rates per fault with the corresponding probable magnitudes of occurrence must be computed for seismic hazard computations in (6). This Section will discuss in detail all the steps that are needed to model the size uncertainty and compute the activity rates.

5.1. Maximum Magnitude Determination

There are five methods used by Valentini, Visini, and Pace [25] and Valentini et al. [24], based on the FiSH Code, a MATLAB Code made by Pace, Visini, and Peruzza [41], to determine the maximum magnitude to be considered in each active fault source model. The following summarizes each method and the steps needed to obtain the maximum size:

Method 1: The average annual displacement was taken with the minimum and maximum slip rates given in Table 2. Then, this displacement and area A

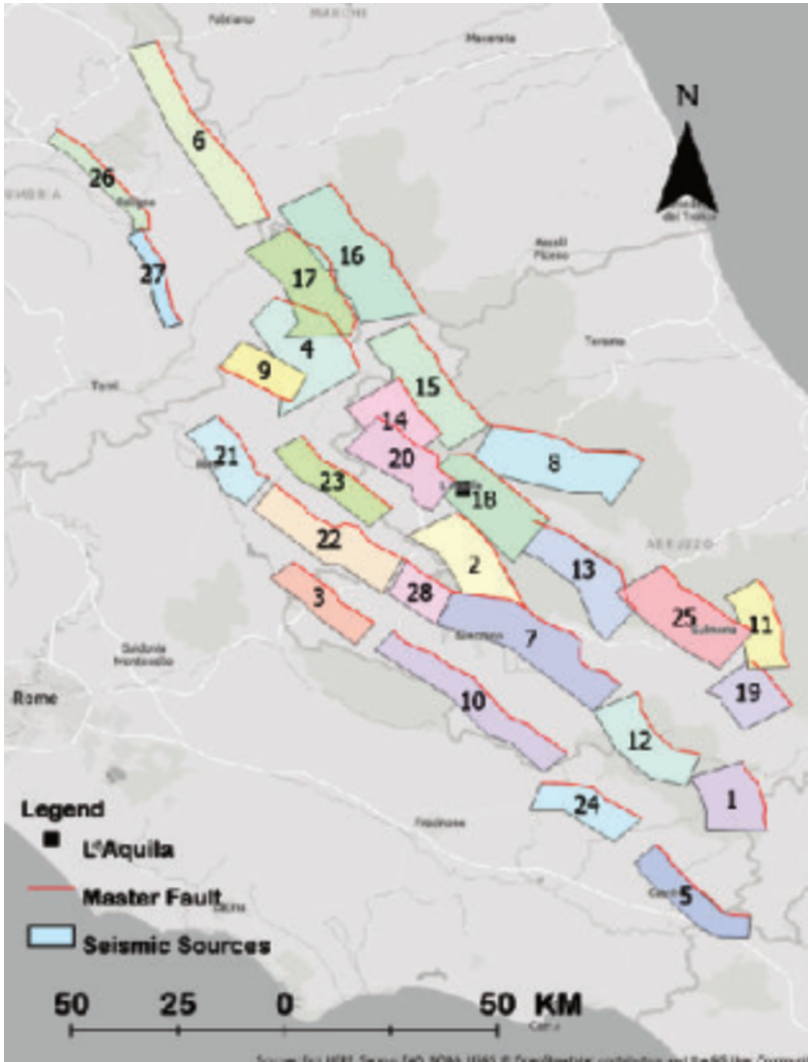


Figure 19. Active fault sources with corresponding master fault traces [25]

(which can be computed from the seismogenic thickness, dip angle, and length as per Subsection 2.3) were used to compute the seismic moment based on the formula in (7), and converting the seismic moment in units of N-m. Then, the moment magnitude is calculated using (36).

Method 2: Given the rupture length L and area A , the maximum earthquake size can be computed using the relationships formulated by Wells and Copper-smith [42] using the global earthquake occurrence data. These are given by:

$$M_w = 5.08 + 1.16L, \quad \sigma_{M_w} = 0.28, \tag{81}$$

$$M_w = 4.07 + 0.98A, \quad \sigma_{M_w} = 0.28. \tag{82}$$

Table 2. Fault parameter needed for PSHA [25]

ID	NAME	Length (km)	Dip (°)	ST (km)	SRmin	SRmax	Mobs	sdMobs	Last eq time
1	Barrea	17.4	50	13	0.2	0.6	-	-	1984
2	Campo Felice-Ovindoli	26.5	50	13	0.7	1.2	-	-	-
3	Carsoli	20.5	50	11	0.35	0.6	-	-	-
4	Cascia-Cittareale	24.2	50	13.5	0.3	0.9	-	-	-
5	Cassino	24.6	60	11	0.25	0.5	-	-	-
6	Colfiorito	45.9	37	8.5	0.25	0.75	6.2	0.33	1997
7	Fucino	38	50	13	0.4	1.4	7.1	0.09	1915
8	Gran Sasso	28.7	50	15	0.6	1	-	-	-
9	Leonessa	14.9	55	12	0.1	0.7	-	-	-
10	Liri	42.5	50	11	0.3	1.26	-	-	-
11	Maiella	21.4	55	15	0.7	1.6	-	-	-
12	Marsicano	20	50	13	0.5	0.7	-	-	-
13	Middle Aternum Valley	29.1	50	14	0.3	0.4	-	-	-
14	Montereale	15.5	50	14	0.3	0.9	-	-	-
15	Mount Gorzano	30	45	12	0.7	1.1	-	-	-
16	Mount Vettore-Mount Bove	34	47	11	0.35	1.05	6.5	0.1	2016
17	Nottoria-Preci	29	50	12	0.3	0.9	6.9	0.11	-
18	Paganica	23.7	50	14	0.45	0.71	6.5	0.34	2009
19	Pizzalto-Cinque Miglia	18	50	15	0.1	0.6	-	-	-
20	Pizzoli-Pettino	21.5	50	14	0.3	0.9	6.7	0.17	1703
21	Rieti	17.6	50	10	0.3	0.5	6.3	0.34	1899
22	Salto Valley	28.4	50	11	0.5	0.7	-	-	668
23	Sella di Corno	28.4	60	13	0.35	0.7	-	-	-
24	Sora	20.4	50	11	0.15	0.45	6.3	0.2	1655
25	Sulmona	22.6	50	15	0.5	0.7	-	-	-
26	Umbra Valley N	28.6	50	4.5	0.4	1.2	6.4	0.1	1832
27	Umbra Valley S	24	50	4.5	0.4	1.2	-	-	1878
28	Velino	11.5	50	12.5	0.7	0.9	5.7	0.1	1904

Method 3: Similarly to Method 2 using the length from Table 2 but modifying it with respect to the aspect ratio of the fault dimensions prediction by Peruzza and Pace [43] as mentioned by Pace, Visini, and Peruzza [41].

Method 4: Lastly, the maximum observed magnitude of occurrence using Table 2 and 3.

Table 3. Historical, Instrumental, Paleoseismological Occurrences in each fault[25, 24]

ID	NAME	Historical				Instrumental		Paleoseismo.
		Date	Io	Mw	sDMw	Date	Mw	Age
1	Barrea					07/05/1984	5.9	
2	Campo Felice-Ovindoli							+890/+1300 3830/3375 7560-4980
3	Carsoli							
4	Cascia-Cittareale	06/11/1599	IX	6.1	0.2			
		16/11/1916	VIII	5.5	0.1			
5	Cassino							
6	Colfiorito	30/04/1279	IX	6.2	0.2	26/09/1997	6.0	
7	Fucino	13/01/1915	XI	7.0	0.1			+426/+782 3500-3300 5944-5618
8	Gran Sasso							3381/+1000 6573/5475
9	Leonessa							
10	Liri							
11	Maiella							
12	Marsicano							
13	Middle Aternum Valley							200/100 BCE 6381/3511
14	Monte reale							
15	Mount Gorzano	07/10/1639	X-XI	6.2	0.2			8320/+1000
		28/04/1646	IX	5.9	0.4			8245/8365
16	Mount Vettore-Mount Bove					30/10/2016	6.5	+250/+450 -2200/-1800 -3700/-2800 -6000/-4000
17	Nottoria-Preci	01/12/1328	X	6.5	0.3	19/09/1979	5.8	+1400/+1800 -500/-50
		14/01/1703	XI	6.9	0.1			
		27/06/1719	VIII	5.6	0.3			
		12/05/1730	IX	6.0	0.1			
		22/08/1859	VIII-IX	5.7	0.3			
		23/02/1879	VIII	5.6	0.3			
18	Paganica	27/11/1461	X	6.5	0.5	06/04/2009	6.3	+890/+1150 -760/+670 -2900/-760
19	Pizzalto-Cinque Miglia							-800/+1030 5685/4890

Table 4. Table 3 continued [25, 24]

Note: +/- indicates the year in CE/BCE, years are presented from the latest to earliest earthquake occurrence, each row representing the start and end years of possible earthquake activity

ID	NAME	Historical				Instrumental		Paleoseismo.
		Date	Io	Mw	sDMw	Date	Mw	Age
20	Pizzoli-Pettino	02/02/1703	X	6.7	0.1			1400/1800
21	Rieti	01/12/1298	IX-X	6.3	0.5			
22	Salto Valley	09/09/1349	IX	6.3	0.1			
23	Sella di Corno							
24	Sora	24/07/1654	X-XI	6.3	0.1			
25	Sulmona							+80/+240 4500 8450/6315 after 9000
26	Umbra Valley N	13/01/1832 12/02/1854	X VIII	6.4 5.6	0.1 0.3			
27	Umbra Valley S	05/06/1767 15/09/1878	VII-VIII VIII	5.5 5.5	0.4 0.2			
28	Velino	24/02/1904	IX	5.7	0.1			-1400/1000

The FiSH code then will take the *average* of all the four values of M_{max} in methods 1-3, and the PDFs of each magnitude value centered at the predicted M_{max} which follows the normal distribution are summed up, and the new PDF is fitted to a normal curve centered at the average of the four values with a new standard deviation sDM_{max} . The criteria to select M_{max} are as follows [24]: a) if $M_{obs} + sDM_{obs}$ is lower than $M_{max} - sDM_{max}$, then use M_{max} . b) if $M_{obs} - sDM_{obs}$ is larger than $M_{max} + sDM_{max}$, then the fault geometries and historical seismicity are reviewed. c) if $M_{obs} + sDM_{obs}$ is within the range of $M_{max} \pm sDM_{max}$, then M_{obs} is used with the given sDM_{obs} in Table 2. Take note that this selection is only valid if there is an observed earthquake. Otherwise, M_{max} predicted by the FiSH code will be used.

5.1.1. Earthquake Recurrence

The recurrence of earthquakes in a certain region can be modeled by the *Guttenberg-Richter* (G-R) Relationship [1, 32] and is given by:

$$\log \lambda_m = a - bM, \quad (83)$$

where λ_m is the mean annual rate of exceedance of earthquakes (in earthquakes/yr) of magnitude M , a is the slope of the regression line related to the activity rate of earthquakes, and b is called the *b-value* of a region which is the relative likelihood of large and small earthquakes. This can be interpreted as an increase in the number of large earthquakes compared to small earthquakes with

the decreasing *b-value*. According to McGuire [15], this *b-value* ranges from 0.7 to 1.1; according to Shearer [32], the value ranges from 0.8 to 1.2; and 0.7 to 1.3 according to Kramer and Scawthorn [2]. In the papers of Valentini et al. [25, 24] the assumed value was 1.0.

This equation was introduced by Gutenberg and Richter in 1944, as mentioned by Kramer [1] and they performed regression analysis for the magnitude size and their annual frequencies in Southern California.

Manipulating (83) and with a change of the base, it can be rewritten into:

$$\lambda_m = v_o \exp(-\beta M), \quad (84)$$

where $v_o = 10^a$ and $\beta = 2.303b$. It can be seen from (84) that the magnitude can go from $-\infty$ to $+\infty$ which is not possible. Then (84) has to be bounded with a minimum value and a maximum value, with a minimum value of 4.0 to 5.0 for engineering purposes [1], and a maximum value which is dictated by the properties of the fault such as geometry, slip rates, etc. Valentini et al. [24] used a *truncated G-R model* (TGR) which utilizes minimum M_o and maximum M_u and is given by:

$$\lambda(m) = \lambda_o \frac{\exp(-\beta m) - \exp(-\beta M_u)}{\exp(-\beta M_o) - \exp(-\beta M_u)}, \quad (85)$$

where $\lambda(m)$ is the mean annual rate of exceedance as a function of magnitude m , λ_o is the smoothed rate of earthquakes at $M_w = 5.5$, and $\beta = 2.303b$. The resulting probability distribution of the truncated G-R can be expressed in terms of the *cumulative distribution function (CDF)*:

$$F_M(m) = P[M < m | m > M_o] = \frac{\lambda(M_o) - \lambda(m)}{\lambda(M_o)} = \frac{\exp(-\beta M_o) - \exp(-\beta m)}{\exp(-\beta M_o) - \exp(-\beta M_u)}, \quad (86)$$

and the corresponding PDF is given by:

$$f_M(m) = \frac{d}{dm} F_M(m) = \frac{\beta \exp(-\beta m)}{\exp(-\beta M_o) - \exp(-\beta M_u)}. \quad (87)$$

The TGR model for an earthquake recurrence to characterize the uncertainties in the size of earthquakes if there is insufficient data about the activity of the fault. However, if there is evidence of fault movements, then a *characteristic earthquake model* can be used.

To compute the activity rates using the TGR model, simply substitute the magnitude of consideration to (85) given the value of the parameter λ_o and the result is interpreted as the activity rate of the fault having a magnitude of m or greater.

For this study, a minimum magnitude of 5.5 and maximum magnitude $M_u = M_{max}$ for each fault was used for the TRG Model of Magnitude Distribution,

and a binning scheme of 0.1 was used. As mentioned before in Section 1, the activity rates were obtained from the link in the Supporting Information mentioned by Valentini et al. [24].

6. Characteristic Earthquake Model

The characteristic earthquake model can be used with evidence of a paleoseismic movement of faults, which suggests that in a certain number of years called the *return period* or *mean recurrence time* (T_{mean}), that the fault will produce a similar magnitude (within ± 0.5 from the maximum magnitude) which is called the *characteristic earthquake* [1].

To estimate T_{mean} , Valentini, Visini, and Pace [25] and Valentini et al. [24] used the method of Field et al. [44] which is given by:

$$T_{mean} = \frac{1}{CharRate} = \frac{10^{1.5M_{max}+9.1}}{\mu DLW}, \quad (88)$$

where $CharRate$ is the mean annual rate of occurrence of a characteristic earthquake, M_{max} is the computed mean maximum magnitude in a fault, μ is the shear modulus, D is the average long term displacement, and L and W are the length of the fault segments along the direction of strike and the downdip width of the fault, respectively. This length may not be the total length of the fault, but only a part of the entire fault [32].

Theoretically, the probability distribution of magnitude is uniform for a characteristic earthquake, nonetheless, some literature employs the use of a truncated normal distribution with the value of magnitude within the range $M_{max} \pm sDM_{max}$ with a binning scheme of 0.1 [24, 25]. The equation of a normal curve for the magnitude PDF is given by:

$$f_M(m) = \frac{1}{\sigma M_{max} \sqrt{2\pi}} \exp\left(-\frac{[m - M_{max}]^2}{2sDM_{max}^2}\right). \quad (89)$$

To compute the activity rates using the Characteristic Earthquake Model, Valentini, Visini, and Pace [25] and Valentini et al. [24] used the Characteristic Brownian Passage Time (CHPBT) model which is a Gaussian curve according to the PDF [24, 45, 41]:

$$P(t) = \sqrt{\frac{T_{mean}}{2\pi\alpha^2 t^3}} \exp\left[-\frac{(t - T_{mean})^2}{2T_{mean}\alpha^2 t}\right], \quad (90)$$

where T_{mean} is obtained from (88), α is the Coefficient of Variation equal to the ratio of the standard deviation of T_{mean} which can be obtained through slip rates [24, 41], and t is the time (in years) of the last earthquake observed in a fault.

For each of the magnitudes in the interval $[M_{max} - sDM_{max}, M_{max} + sDM_{max}]$, a fictitious recurrence time T_{fict} is computed for a given magnitude, and is given by:

$$T_{fict} = \frac{1}{\lambda_m} = \frac{-\Delta T}{\ln(1 - P|_{elap})}, \quad (91)$$

where λ_m is the activity rate of the fault having a magnitude of m or greater, ΔT is the selected observation period (depending on the design life of a structure typically set for 50 years) and $P|_{elap}$ is the conditional probability that an event occurs during the next ΔT year, given an elapsed time T_{elap} since the last event, is defined as follows:

$$P|_{elap} = P(T_{elap} \leq T + T_{elap} + \Delta T | T > T_{elap}) = \frac{P(T_{elap} \leq T \leq T + T_{elap} + \Delta T)}{1 - P(0 \leq T \leq T_{elap})}, \quad (92)$$

for which the expressions in the numerator and the denominator of the RHS of (92) can be obtained by numerically integrating (90) with the corresponding bounds $T_{elap} \leq T \leq T + T_{elap} + \Delta T$ and $0 \leq T \leq T_{elap}$ for the numerator and the denominator, respectively. This probability in (92) is set to the probability considering a Poisson process with parameter $\lambda = 1/T_{fict}$ and $t = \Delta T = 50$ years. Figure 20 illustrates the concept used by the CHBPT model of computing the activity rates of earthquakes.

Hence, the following is employed in this study: a) the TGR model is used for fault sources that have no data regarding the last earthquake occurrence from Table 2; b) in the case that the active fault sources have earthquake associations based on Table 3, the TGR is used; if there is at least one earthquake having a magnitude lower than the magnitude range for the CHBPT, c) otherwise, the CHBPT is used. Both b) and c) are with reference to Valentini et al. [24].

In determining the values of the earthquake parameters related to the magnitude PDF, the results from Valentini, Visini, and Pace [25] and Valentini et al. [24] are used in this study.

Table 5 lists the maximum magnitude M_{max} and its standard deviation sDM_{max} , mean recurrence time T_{mean} (in years), the coefficient of variation COV , and the time elapsed T_e (in years). For some faults with no observed earthquakes according to Table 3, an assumed value of 717 years was used as per the assumption of Valentini et al. [24] which is the minimum number of years of recording of earthquakes. The values listed in Table 5 were used to calculate the seismic moment M_o by multiplying the seismic moment rate to the mean recurrence time, and this seismic moment can be correlated to the energy released during earthquakes and the dynamic stress drop which describes the total change in stress during earthquakes as mentioned in Section 2.3 of this paper.

It follows from Table 5, that the Velino fault has the lowest maximum magnitude of 6.1, while the Fucino and Liri faults have the highest maximum magnitude of 6.8, which were determined using the four methods mentioned in Subsection 5.1. The values of the standard deviations for each maximum magnitude of each fault were determined from the four methods as well, the

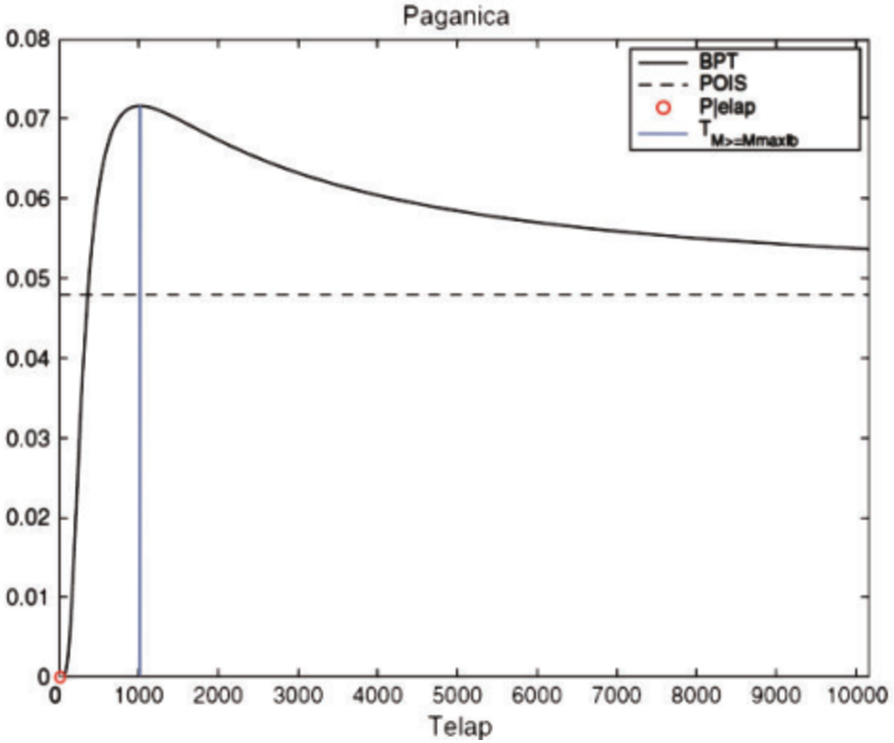


Figure 20. A CHBPT model was employed for the Paganica Fault showing the BPT probability values for each value of $t = T_{elap}$. $P|_{elap}$ in (91) obtained from BPT in (89) is computed for a given T_{elap} , and this probability is equated to the Poisson probability corresponding to 50 years of observation with a parameter equal to $1/T_{fict}$ which is the mean occurrence rate corresponding to a given magnitude and T_{mean} which are related by (87)[41]

values of which were used for the CHBPT models to determine the upper bound of the magnitude range for determining the activity rates.

The mean recurrence time T_{mean} was determined using (87), and other parameters such as CV and seismic moment rates were obtained from the FiSH Code calculations made by Valentini et al. [24]. Some values of the elapsed time were obtained from the study of Valentini et al. [24], and for those seismic sources that were not considered in their study, a value of 717 years was assumed as mentioned by Valentini et al. [24] which is the minimum required number of years of recording for an earthquake catalogue to be complete.

7. Physics-Based Ground Motion Prediction

The PGA can be approximated by simulating a ground motion by solving the Elastodynamic Equation with the Hooke's Law in (40) the approximation of which is given by (63) using the finite difference method in a staggered grid, given the initial and boundary data in Subsection 3.2.1.

The Preliminary Reference Earth Model (PREM) was used in this study for the density and S-wave velocity of rock which assumes a 1-D model of the Earth's seismic velocities [32]. For the computation of normal stresses, a dry density of 2.60 g/cc was used from this model and this assumes depths of several kilometers from the ground surface. The S-wave velocity used was taken from the same model and is equal to 3.2 km/s.

The parameters required for the boundary condition for the traction such as the rupture velocity v_r , the rupture time t_r , the fracture energy G , the dynamic stress drop $\Delta\sigma_d$, and the characteristic time t_1 were calculated in each magnitude of the occurrence per fault, ranging from M_{min} to M_{max} . Seismic moments were computed by multiplying the seismic moment rate to the mean recurrence time. For each magnitude, seismic moments were interpolated from M_{max} using the relation of the moment magnitude and the seismic moment in (8).

The domain for the computational framework is $[0, L_p] \times [0, T]$, where L_p is the length obtained from the binning in Subsection 4.2 for distances, T for the seismogram duration, which was 10 sec plus the time which it takes for the S-wave to reach the site, which is given by L_p/β , since at the time before L_p/β , there is no ground motion produced for the site to perceive it. For this study, a uniform time step of $\Delta t = 0.005$ sec was used which is a typical time step in a true seismogram. Then, a uniform grid spacing of 20 m was used making the CFL number equal to 0.80 which satisfies the stability and convergence of the numerical scheme. This spacing is chosen with conservatism, for which the actual ground motions data obtained from the Engineering Strong Ground Motion Database [46] was simulated using the numerical scheme. The ground motions used came from the M_w 6.1 L'Aquila and M_w 6.5 Central Italy earthquakes which occurred on April 6, 2009 and October 30, 2016, respectively.

For the PGA calculations, a Matlab Script is provided in Appendix C to this paper. All the important parameters related to the simulation were computed in MS Excel.

All possible lengths L_p from Subsection 4.2 were considered, and the resulting seismograms were transformed into acceleration vs. time by taking the slope of velocity-time plots in each time step, assuming no acceleration at the beginning of the simulation. Then, the peak values of the acceleration for each magnitude-distance pair were obtained for all seismic sources. These PGAs are grouped according to their respective magnitude of the occurrence and the propagation distance, and the corresponding probability of exceedance $P[Y > y | rup_n]$ of a PGA value given its distance and magnitude were computed by taking the total number of distances whose PGA Y was greater than a reference PGA y for hazard calculations ($N[R_{Y>y}]$), divided by the total number of distances in each fault, which is $N_R = 100$. Mathematically, this is given by:

$$P[Y > y | rup] = \frac{N[R_{Y>y}]}{N_R}. \quad (93)$$

Table 5. Maximum Magnitude and its standard deviation, mean the recurrence time (in years), the coefficient of variation, the time elapsed (in years), and the seismic moment rate (in N-m/yr) [24]. * means that an assumed value of 717 years is used for complete years of recording as per the assumption in their study

id	Name	Mmax	sdMmax	T_{mean} (years)	COV	T_{elap} (yrs)	Seismic Moment Rate (N-m/yr)
1	Barrea	6.3	0.3	1001	1.15	35	3.54E+15
2	Campo Felice Ovindoli	6.6	0.2	851	0.74	702	1.18E+16
3	Carsoli	6.4	0.2	1195	0.74	717*	4.19E+15
4	Cascia Cittareale	6.5	0.2	922	0.85	717*	7.68E+15
5	Cassino	6.5	0.2	2611	0.77	717*	2.71E+15
6	Colfiorito	6.4	0.2	1245	0.85	22	4.40E+15
7	Fucino	6.8	0.3	1791	1.18	104	1.11E+16
8	Gran Sasso	6.7	0.3	1090	1.07	3419	1.30E+16
9	Leonessa	6.2	0.3	959	1.28	717*	2.62E+15
10	Liri	6.8	0.3	2822	1.2	717*	7.07E+15
11	Maiella	6.5	0.2	524	0.79	717*	1.35E+16
12	Marsicano	6.5	0.2	1104	0.71	717*	6.11E+15
13	Middle Aternum Valley	6.6	0.2	2009	0.71	2219	4.98E+15
14	Monte reale	6.3	0.3	696	1.15	717*	5.10E+15
15	Mount Gorzano	6.6	0.2	898	0.73	380	1.11E+16
16	Mount Vettore Mount Bove	6.7	0.3	2042	1.15	3	6.92E+15
17	Nottoria Preci	6.6	0.3	1173	0.7	316	6.39E+15
18	Paganica	6.5	0.2	1113	0.73	10	7.54E+15
19	Pizzalto C Miglia	6.5	0.2	1354	1.26	989	3.70E+15
20	Pizzoli-Pettino	6.5	0.2	1001	0.85	316	7.07E+15
21	Rieti	6.3	0.3	1294	1.07	721	2.76E+15
22	Salto Valley	6.5	0.2	1302	0.71	668	5.17E+15
23	Sella di Corno	6.5	0.2	1370	0.77	717*	5.17E+15
24	Sora	6.4	0.2	1939	0.85	365	2.64E+15
25	Sulmona	6.5	0.2	855	0.71	1919	7.96E+15
26	Umbrea Valley N	6.3	0.4	2411	1.47	187	1.47E+15
27	Umbrea Valley S	6.2	0.4	1707	1.47	141	1.47E+15
28	Velino	6.1	0.3	395	1.04	115	4.50E+15

The reference PGAs (in terms of g 's) used for this study were as follows: 0.01 to 0.09 (in multiples of 0.01) and 0.10 to some upper limit, which is the maximum predicted PGA for all rupture scenarios.

8. Seismic Hazard Calculations

Hazard calculations were based on Tarbali et al. [19] and Tarbali et al. [20] which are rupture-based scenarios, and for this study it is the magnitude occurrence in the fault source. The probability of exceedances was computed based on the frequencies of the predicted PGA as a function of the distance given the magnitude of the occurrence.

From (6), the hazard rate of exceedance overall rupture scenarios in all seismic sources assuming that the sources are independent of each other and collectively exhaustive, is given by

$$\lambda_{IM}(im) = \sum_{n=1}^{N_{rup}} P[Y > y | rup_n] \lambda_{Rup}(rup_n), \quad (94)$$

where $P[Y > y | rup]$ is the probability of exceedance in (93), $\lambda_{Rup}(rup_n)$ is the hazard rate of the given rupture scenario (magnitude of occurrence) which is the probability of occurrence of the magnitude multiplied to the activity rates in a given magnitude.

A series of reference PGA values were used to construct the *hazard curve*, the plot of PGA values vs. the hazard rate or the mean annual rate of exceedance for a given site [1], which is L'Aquila in this study.

9. Modeling of Temporal Uncertainty

The occurrence of earthquakes is assumed to follow the Poisson distribution [1], and is given by

$$P[\lambda, t, n] = \frac{(\lambda_{IM}t)^n e^{-\lambda_{IM}t}}{n!}, \quad (95)$$

where λ_{IM} is the mean annual rate of exceedance of earthquakes (in earthquakes/yr), t is the observation time (in years), and n is the number of earthquakes. This model assumes an average number of earthquakes $\mu = \lambda_{IM}t$ occurring given a certain magnitude of earthquake at any time and obtains the probability of a certain number of occurrences.

It is known that the Poisson distribution has an assumption that the events are rare and random, and since earthquake occurrences are rare, therefore many analysts in the past till the present would assume Poisson arrivals of earthquakes. This model is used to account for the uncertainty in time, since earthquakes may recur at different time intervals. Also, the events must be independent in space, size, and time. Therefore, it is very important that earthquakes are classified as main events and not foreshocks and aftershocks, which is the reason why their occurrences are consistent with the Elastic Rebound Theory.

9.1. Probability of Exceedance

The probability of exceedance (PE) refers to the probability of exceeding zero earthquakes during an observation period given a certain magnitude of interest [10, 1], which is set to 5.5 for this study. Following the assumption of a Poisson process, using (95), the probability of zero earthquakes is $e^{-\lambda_{IM}t}$. Hence, the probability of exceeding zero earthquakes, is the complement of the event of zero earthquakes, and is given by

$$PE = 1 - e^{-\lambda_{IM}t}. \quad (96)$$

9.2. Seismic Hazard Rate and Return Period

Earthquakes are quantified in terms of their hazard rates λ_{IM} or known as the mean annual rate of exceedance [15, 1] as mentioned before. This hazard rate is obtained from equation (6), which is the direct application of the PSHA Methodology. The time of exposure (T) is the observation period mentioned in (95), which is defined as the number of years for which a structure must withstand a certain kind of earthquake and its corresponding ground motion [22].

The return period (RP) is the inverse of the hazard rate with units of years/earthquake, and the design codes express the desired ground motion for the design as a function of the return period [10]. Using (96), the return period, the time of exposure and the probability of exceedance can be related:

$$PE = 1 - e^{-T/RP}. \quad (97)$$

According to the building code, it is recommended that a structure must withstand a reference PGA which corresponds to a reference probability of exceedance of 10% within 50 years of life of a structure such as a building or a house or commercial establishment. However, a lower probability of exceedance is required for dams, bridges, power plants or lifelines [22]. Valentini, Visini, and Pace [25] and Valentini et al. [24] calculated the PGA in two return periods of 475 and 2475 years, with the corresponding probability of exceedance in 10% and 2%, respectively. Hence for this study, the return periods of 475 and 2475 years were also obtained.

10. Application of PSHA: Elastic Design Spectrum

When the structure experiences the ground acceleration at its strongest shaking, this acceleration is termed spectral acceleration (S_d) [1, 2] or pseudo-acceleration [47, 48]. This quantity has units of gals (cm/s^2) or may be expressed in terms of the gravitational acceleration constant g . It is desirable to express the ground shaking it experiences in terms of its spectral acceleration because this is the ground acceleration experienced by a structure depending on its natural period and damping mechanism [14]. Also, spectral acceleration can be used to calculate the base shear in structures [47, 48]. For many seismic hazard analyses, it is much more convenient to express the impact of the ground shaking in terms

of the spectral acceleration as they are used to calculate the design loads on the structure.

In a seismic design of structures, a structure is characterized by its *fundamental natural period* T (measured in seconds), which is the period that it takes for a structure to have a complete oscillation during vibrations [47, 48]. A structure is said to be a *short-period structure* if the period is less than one second, while structures with a period greater than or equal to one second are called *long-period structures*.

The peak ground acceleration (PGA) or peak horizontal acceleration (PHA) is the ground acceleration which corresponds to the spectral acceleration at the zero natural period [1]. When it comes to risk mitigation, it is desirable to report the impact of ground shaking in terms of PGA, since this will be the ground acceleration that will be experienced by people when an earthquake hits a certain region. This quantity may be also expressed in gals or in terms of g . Usually, this quantity can be measured by instruments called accelerographs during earthquakes. Kramer [1] said that PGA was the geometric mean of the peak of horizontal components of the ground motion.

In Eurocode 8, a reference PGA a_{gR} is desired to construct the so-called *Elastic Design Spectrum* as shown in Figure 21 [22] to estimate the spectral acceleration for a given natural period of a structure. The PGA is extracted from the hazard curve constructed in the PSHA, with the corresponding desired return period of earthquakes, and this PGA is called the *reference* PGA.

From Figure 21, the elastic response spectrum $S_d(T)$ is defined as

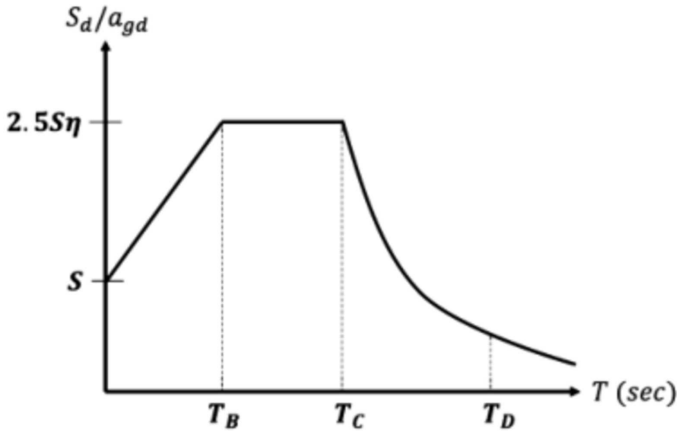


Figure 21. Elastic Design Spectrum for Seismic Design of Structures [22]

where S_d is the design spectral acceleration, $a_{gd} = \gamma a_{gR}$ is the design PGA, a_{gR} is the reference PGA from the hazard curve, γ is typically set to 1.0, S is the soil factor related to the available geotechnical investigations (set to 1.0) for rocks, T is the natural period of the structure, η is a parameter related to damping typically

set to 1.0 for 5% viscous damping of structures, $T_B = 0.15$ sec, $T_C = 0.40$ sec, and $T_D = 2.0$ sec, considering the ground motion is generated by a magnitude of 5.5 and above.

Making an elastic response spectrum for the engineering design of structures is a direct application of the PSHA, and therefore the PSHA must be conducted with care, considering all the factors required for calculating the seismic hazard. The more data is present, the better the estimation of the seismic hazard level on a site.

REFERENCES

- [1] Kramer S L 1996 Geotechnical earthquake engineering, Prentice-Hall Inc, New Jersey 1
- [2] Kramer S L and Scawthorn C 2000 Geotechnical earthquake considerations, Bridge Engineering Handbook, Wai-Fah Chen and Lian Duan. Boca Raton: CRC Press, 132
- [10] Cornell C A 1968 Engineering seismic risk analysis, Bulletin of the Seismological Society of America 58 1583
- [14] Bazurro P and Cornell A C 1999 Disaggregation of seismic hazard, Bulletin of Seismo-logical Society of America 89 501
- [15] McGuire R K 1995 Probabilistic seismic hazard analysis and design earthquakes: closing the loop, Bulletin of the Seismological Society of America 85 1275
- [19] Tarbali K, Bradley B, Huang J, Polak V, Lagrava D, Motha J, and Bae S 2018 CYBERSHAKE NZ V179: New Zealand simulation-based probabilistic seismic hazard analysis, 16th European Conference on Earthquake Thessaloniki Engineering
- [20] Tarbali K, Bradley B, Huang J, Lee R, Lagrava D, Bae S, Polack V, Motha J, and Zhu M 2019 CYBERSHAKE NZ V185: New Zealand simulation-based probabilistic seismic hazard analysis, 2019 Pacific Conference on Earthquake Engineering - New Zealand Society for Earthquake Engineering
- [22] Solomos G, Pinto A, and Dimova S 2008 A Review of The Seismic Hazard Zonation in National Building Codes in the Context of Eurocode 8, European Commission, Varese Italy, Joint Research Center JRC Technical Report
- [24] Valentini A, Pace B, Boncio P, Visini F, Pagliaroli A, and Pergalani F 2019 Definition of seismic input from fault-based PSHA: Remarks after the 2016 Central Italy earthquake sequence, AGU 100: Advancing Earth and Space Science
- [25] Valentini A, Visini F, and Pace B 2017 Integrating faults and past earthquakes into a probabilistic seismic hazard model for peninsular Italy, Natural Hazards and Earth System Sciences 17 (11) 2017
- [32] Shearer P 2009 Introduction to Seismology 2nd ed, Cambridge University Press, New York
- [41] Pace B, Visini F, and Peruzza L 2016 FiSH: MATLAB tools to turn fault data into seismic-hazard models, Seismological Research Letters 872A 374
- [42] Wells D, and Coppersmith K 1994 New empirical relationships among magnitude, rupture length, rupture width, rupture area and surface displacement, Bulletin of the Seismological Society of America 90 73
- [43] Peruzza L and Pace B 2002 Sensitivity analysis for seismic source characteristics to probabilistic seismic hazard assessment in central Apennines (Abruzzo area), B. Geofis. Teor. Appl. 11 79
- [44] Field E H, Jackson D D and Dolan J F 1999 A mutually consistent seismic-hazard source model for southern California, Bulletin of Seismological Society of America 89 559
- [45] Matthews M V, Ellesworth W L, and Reasenber P A 2002 A Brownian model for recurrent earthquakes, Bulletin of the Seismological Society of America 92 (6) 2233
- [46] Luzi L, Lanzano G, Felicetta C, D'Amico M C, Russo E, Sgobba S, Pacor, F and ORFEUS Working Group 5 2020 Engineering Strong Motion Database (ESM) (Version 2.0), Istituto Nazionale di Geofisica e Vulcanologia (INGV)
- [47] Paz M, and Leigh W 2004 Structural dynamics: Theory and computation, 5th ed, Kluwer Academic Publishers Group, Massachusetts
- [48] Chopra A K 2001 Dynamics of structures: Theory and applications to earthquake engineering, Prentice Hall Inc., New Jersey